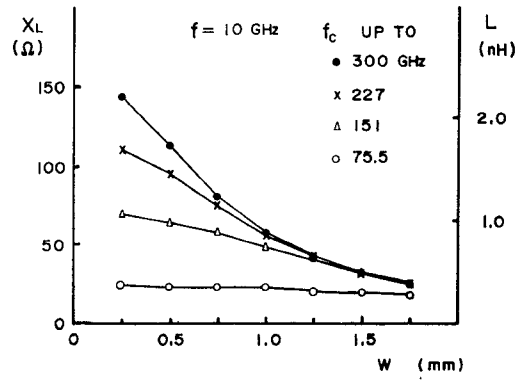

Fig. 6 The conductor strip inductance versus the strip width The inductance is evaluated by truncating the series at 75.5 GHz through 300 GHz with respect to the eigenvalues and holding $n < 4$ with respect to the spatial harmonics Ordinate: inductance L, in nanohenries Abscissa: strip width w, in millimeters.

discussions given in [6] would apply to our problem, and that the series converges for finite w and g. However, our study is incomplete at the time of this writing, and our approach here is to calculate the values of the inductance at various values of the strip width w, using different numbers of the eigenvalues while holding $n \leq 4$ as a test of convergence. A typical set of results are presented in Fig. 6, where all the relevant eigenvalues up to 75.5 GHz through 300 GHz that were detected by a numerical method of scanning on the computer were used. Since the numerical method of scanning has the possibility of leaving out some eigenvalues undetected, precaution is required to include most of the eigenvalues, particularly those of the lower order modes. This is done by checking the number of the eigenvalues detected against that estimated for the through region rectangular waveguide and also by identifying the modes for some twenty lowest order modes.

Fig. 6 shows that truncation at about 300 GHz is acceptable for $w \geq 1.00$ mm. As the width decreases, an increasingly large number of eigenvalues will be required for precision analysis.

Conclusions

A simplified model of the ridged-waveguide mounting structure has been analyzed theoretically. The ribbon-and-pedestal of the microwave diode was represented by an equivalent flat conductor strip having an equivalent width, an infinitesimal thickness, and a gap. The conductor strip was regarded as a small antenna and its driving-point impedance was derived using the induced EMF method. The dyadic Green's function for the ridged waveguide was also derived to facilitate the analysis. The results of the analysis were represented by an equivalent circuit that involved infinite array of transformers representing the couplings between the spatial harmonic components of the current in the conductor strip and the waveguide normal modes. The equivalent circuit was reduced to a simple one convenient for use in practical designs and analyses of microwave circuits involving the mount of this type. Numerical results for a typical example were given to discuss the validity of the theoretical results and also to demonstrate a remarkably smooth behavior of the driving-point impedance of the mount over a frequency range from 5.4 to 25.4 GHz.

The neglect of the package ceramic ring and the lack of theoretical procedure of defining the equivalent width of the flat conductor strip were major shortcomings of the analysis. Experimental measurements were required to supplement these aspects. A through discussion on the convergence properties of the summation was also left for future study. However, the results presented in this short paper will be useful for designs and analyses of various microwave components and circuits involving small devices such as Gunn and IMPATT diodes as well as for characterization of these devices over a wide range of frequencies.

References

[1] D. H. Claxton and P. T. Greiling, "Broad-band varactor-tuned IMPATT-diode oscillator," *IEEE Trans. Microwave Theory Tech.*, vol MTT-23, pp. 501–504, June 1975

[2] P. J Meier, "Integrated fin-line millimeter components," *IEEE Trans. Microwave Theory Tech*, vol. MTT-22, pp. 1209–1216, Dec 1974

[3] S. Mizushina and T. Ohsuka, "The ridged-waveguide-cavity Gunn oscillator for wideband tuning," *IEEE Trans Microwave Theory Tech*, vol MTT-24, pp 257–259, May 1976.

[4] H. Kondoh, S Mizushina, and N Kuwabara, "Broad-band IMPATT and Gunn oscillators with ridged-waveguide cavity," Inst. Elect. Communication Engr Japan Tech. Rep, MW-76-130, Jan. 1977

[5] E. Yamashita and J R Baird, "Theory of tunnel diode oscillator in a microwave structure," *Proc IEEE*, vol. 54, pp. 606–611, Apr 1966

[6] R R. Eisenhart and P. J Khan, "Theoretical and experimental analysis of a waveguide mounting structure," *IEEE Trans Microwave Theory Tech*, vol. MTT-19, pp. 706–719, Aug. 1971.

[7] C-T. Tai, *Dyadic Green's Functions in Electromagnetic Theory* Scranton, PA: Intext Educational Publ, 1971, ch 5, pp. 69–80.

[8] J. P. Montgomery, "On the complete eigenvalue solution of ridged waveguide," *IEEE Trans Microwave Theory Tech.*, vol. MTT-19, pp 547–555, June 1971

Application of Gratings in a Dielectric Waveguide for Leaky-Wave Antennas and Band-Reject Filters

TATSUO ITOH, SENIOR MEMBER, IEEE

Abstract—**Grating structures fabricated in inverted-strip dielectric waveguides have been used for the first time as leaky-wave antennas and band-reject filters. They are potentially useful for millimeter-wave integrated circuits. Experimental results agree reasonably well with theoretical predictions.**

I. Introduction

Grating structures are commonly employed in optics as beam couplers [1] and as frequency-sensitive reflectors for distributed-feedback lasers [2]. However, such gratings have not yet been widely used at millimeter wavelengths. Since dielectric waveguides in millimeter-wave integrated circuits (MMIC) are low-frequency replicas of optical waveguide, it is clear that many techniques could be transferred from the optical to the millimeter-wave domain.

This paper reports the first reduction to practice of a frequency-scannable leaky-wave antenna and a band-reject filter made of grating structures implemented in the inverted-strip (IS) dielectric waveguide [3], [4]. The antenna and filter are compatible with, and naturally complement, the directional couplers, oscillators, and phase shifters that have already been developed using dielectric waveguide fabrication techniques [3]–[7]. Grating structures can be easily and economically fabricated in the IS guide. The performance of the antenna and the filter made of gratings can be optimized in a relatively easy and flexible manner. Hence, the development of these devices is likely to contribute to realization

Manuscript received May 19, 1977; revised July 21, 1977.
The author is with the University of Kentucky, Lexington, KY 40506

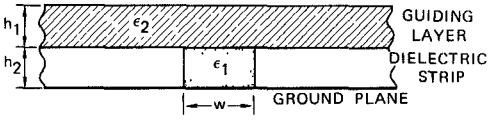

Fig 1. Cross section of IS waveguide

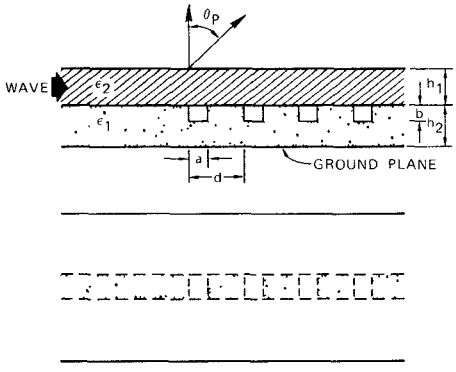

Fig 2. Side and top views of grating configuration in IS waveguide.

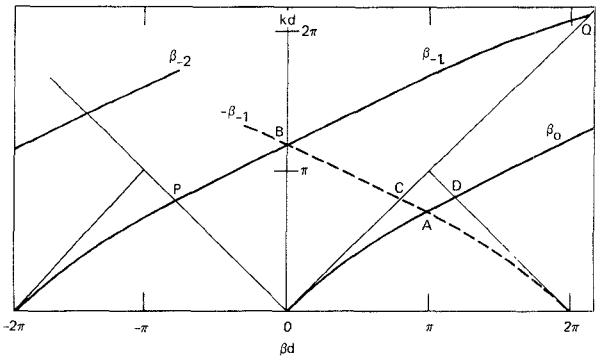

Fig 3. Dispersion characteristics of a number of space harmonics when mode coupling phenomena are neglected. $\varepsilon_1 = 2.1$ (Teflon), $\varepsilon_2 = 3.75$ (Stycast Hik), $h_1 = h_2 = 1.58$ mm, $w = 4$ mm

of high overall performance of millimeter-wave systems with modest cost and effort.

The antenna reported here has a number of useful features. First, since it is planar, it is easy to connect with an RF front end in the form of a microwave integrated circuit or MMIC. Second, it can be flush-mounted on the exterior surface of a large body, such as an aircraft, thus eliminating the need for a radome. The antenna can provide high gain, and its main beam is steerable in almost any angular sector between endfire and backfire directions. Also, the main beam can be shaped by controlling the grating profile.

The band-reject filter is based on the stopband phenomenon exhibited by a grating structure within its nonradiating region. The return loss and bandwidth can be controlled by adjusting the profile and length of the gratings.

The operating principle of, and some of the phenomena exhibited by, a grating created on an open (surface) waveguide such as the IS guide are fundamentally different from those associated with the closed-metal waveguide. Hence, in Section II, the analysis and design of a grating on an IS waveguide are briefly explained. In Section III, measured results using prototype antennas and filters are presented and compared with numerical data. In Section IV, concluding remarks and some suggestions for future work are given. It should be noted that the analysis and design features reported in this paper are quite general and are applicable to several dielectric waveguide structures in addition to the IS.

II. Grating Structures in IS Waveguide

The IS waveguide has a number of useful features. It has low loss, has a ground plane for conveniently mounting solid-state devices, and is easy to fabricate. Unlike many other dielectric waveguides, the major portion of the energy launched into the IS guide, shown in Fig. 1, travels in the planar guiding layer (ε_2) and is also transversely concentrated in the region immediately above the dielectric strip (ε_1). Many functional devices [4] can be created by appropriate choice of the configurations of one or more dielectric strips below the guiding layer, which remains intact.

Gratings can be created by periodically modulating the geometrical or material nature of the dielectric strip and still leaving the guiding layer intact. For instance, as shown in Fig. 2, grooves are created periodically in the dielectric strip. This groove configuration perturbs the transmission characteristics of the IS guide periodically, thereby functioning as a grating.

Electromagnetic waves in a grating region can be represented in terms of space harmonics whose phase constants are

$$\beta_m = \beta_0 + \frac{2m\pi}{d}, \qquad m = 0, \pm 1, \pm 2, \cdots \tag{1}$$

where d is the grating period, and β_0 is the phase constant of the dominant ($m = 0$) space harmonic determined by the excitation of the grating. If perturbation due to each unit cell of the grating is small, β_0 is very close to the phase constant β_{sw} of the dominant surface wave in the unperturbed IS guide, except in a coupling region described later. In this discussion, the effect of higher order surface-wave modes in the IS guide is not considered.

Fig. 3 shows k-β plots for the $m = 0(\beta_0)$, $m = -1(\beta_{-1})$, and $m = -2(\beta_{-2})$ forward-traveling space harmonics, and the $m = -1(-\beta_{-1})$ of the backward-traveling fundamental. The curve for β_0 is reproduced from the dispersion relation of the dominant E_{11}^y mode, β_{sw}, of the IS guide obtained by using the method reported earlier by Itoh [3]. Curves for higher space harmonics are obtained by shifting β_0. Mode coupling phenomena associated with synchronous points such as A, B, C, and D are not shown. When the product of the wavenumber k and the grating period d is chosen such that the phase constant of the pth harmonic (say, $p = -1$) satisfies

$$|\beta_p/k| < 1, \qquad k = \text{free-space wavenumber} \tag{2}$$

the grating supports a leaky wave, and the energy traveling in the grating leaks into free space along the direction $\theta_p = \sin^{-1}(\beta_p/k)$ measured from the broadside of the grating [8]. In Fig. 3, these $\beta_p(p = -1)$ lie on the curve from P to Q except near coupling points such as B, where a mode coupling occurs between different space harmonics. Since these points lie in the radiation region of k-β diagram, the mode coupling is different from that at A, as discussed in the latter part of this section [8]. These coupling points in the radiation region will not be discussed here. However, it is interesting to note that B corresponds to the broadside direction ($\theta_p = 0$). Coupling phenomena at the backfire and endfire points (P and Q) will not be discussed in this paper, either.

We shall now study the power pattern of the radiation from a finitely long grating consisting of N unit cells. If the perturbation due to the unit cell is infinitesimal, and if the operating point is not in one of the coupling regions, the grating structures can be viewed as an N-element linear array of spacing d, illuminated uniformly with a linear phase taper corresponding to β_0. Since the energy loss at each unit cell is assumed small, the amplitude taper

is also small. If we ignore amplitude taper, the radiation pattern can be expressed approximately as

$$|f(\theta)|^2 = \frac{1}{N^2}\left|\frac{\sin(N\Psi/2)}{\sin(\Psi/2)}\right|^2 \tag{3}$$

where $\Psi = kd \sin\theta - \beta_0 d$.

Let us now turn our attention to the stopband phenomenon around point A in Fig. 3. When d is chosen as

$$\beta_0 d = \pi, \qquad \beta_0 \approx \beta_{sw} \tag{4}$$

the grating exhibits a stopband phenomenon. The energy incident on the grating is reflected back at the frequency at which (4) is satisfied.

This stopband results from the mode coupling between the forward-traveling fundamental β_0 and the $m = -1$ harmonic of the backward-traveling fundamental. The dispersion characteristics in the vicinity of this stopband are now derived using an equivalent-circuit representation.

Recognizing that each unit cell of the grating consists of grooved and nongrooved sections, we represent the cell in terms of two cascaded transmission lines of length a and $d - a$, respectively. We assume that junction effects between these two sections are negligible. Imposing a condition that the input and output of each unit cell are identical except for the factor that accounts for the complex phase delay, we obtain the following dispersion relation [9]:

$$\cosh\gamma d = \cos\bar{\beta}_{sw}a\cos[\beta_{sw}(d-a)] + \frac{1}{2}\left(\frac{\beta_{sw}}{\bar{\beta}_{sw}} + \frac{\bar{\beta}_{sw}}{\beta_{sw}}\right)\sin(\bar{\beta}_{sw}a) \cdot \sin[\beta_{sw}(d-a)] \tag{5}$$

where $\bar{\beta}_{sw}$ and β_{sw} are phase constant in the grooved and nongrooved sections of IS guide.

In the stopband, $\gamma = \alpha + j\pi$, where α is real. The width of the stopband can be computed from the frequencies at which the magnitude of the right-hand side of (5) equals one. Note that β_{sw} and $\bar{\beta}_{sw}$ in (5) are in turn related to the frequency via dispersion relations of corresponding IS guide structures. The reflection phenomenon due to stopband is frequency-sensitive; thus a grating can be used as a band-reject filter. The bandwidth and reflectance depend on the grating profile, the length of the grating region, etc.

III. Results and Discussion

A leaky-wave IS guide antenna for 60 GHz was designed. After the design was completed, all the dimensions were scaled by a factor of four to permit experiments at 15 GHz. This scaling is for demonstrating the operating principle with modest cost and time for fabrication. A model antenna is pictured in Fig. 4. Since the guiding layer (Stycast Hik, $\varepsilon_r = 3.75$) is nontransparent for light, a disassembled view was taken. The smaller tip on one end of the guiding layer is the transition region for launching, whereas the larger tip on the other end is to avoid the reflection of energy left unradiated at the grating.

Fig. 5 shows measured and computed (using (3)) radiation patterns of the model antenna. At 15 GHz, the main beam is directed $-26°$ ($26°$ toward the backward direction) from the broadside, while at 17 GHz the main-beam direction is $-10°$ from the broadside. Measured and computed sidelobe levels are -10 dB and -13 dB, respectively, at the two frequencies.

Notice that (3) describes only the array pattern, whereas measured patterns automatically include any directional scattering characteristics of the unit cell. Since the measured pattern and the computed array pattern agree well, scattering from each cell is found to be not highly directive.

The largest discrepancy between the theoretical and experimental results occurs in the forward direction. The major reason is that the model antenna is not long enough. Since the number of grating elements is small, considerable electromagnetic energy is

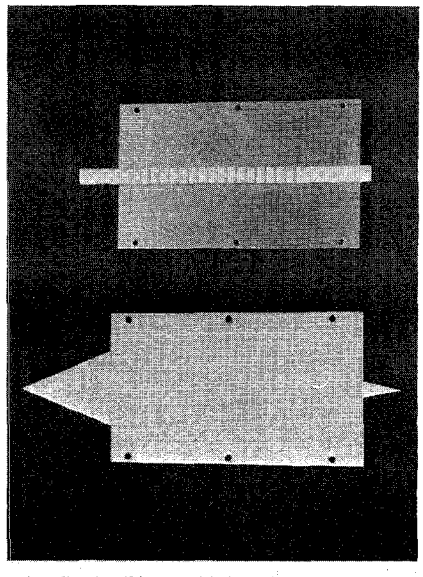

Fig. 4. Disassembled grating antenna.

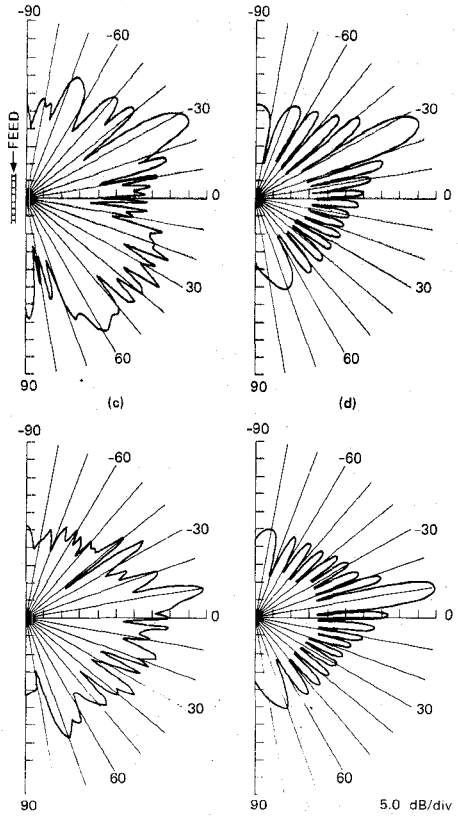

Fig. 5. Radiation patterns of grating antenna. $d = 10.16$ mm, $a = 3.18$ mm, $b = 4.76$ mm, $h_1 = h_2 = 6.35$ mm, $\varepsilon_1 = 2.1$ (Teflon), $\varepsilon_2 = 3.75$ (Stycast Hik), number of grating elements is 17. (a) Measured at 15 GHz. (b) Computed at 15 GHz. (c) Measured at 17 GHz. (d) Computed at 17 GHz.

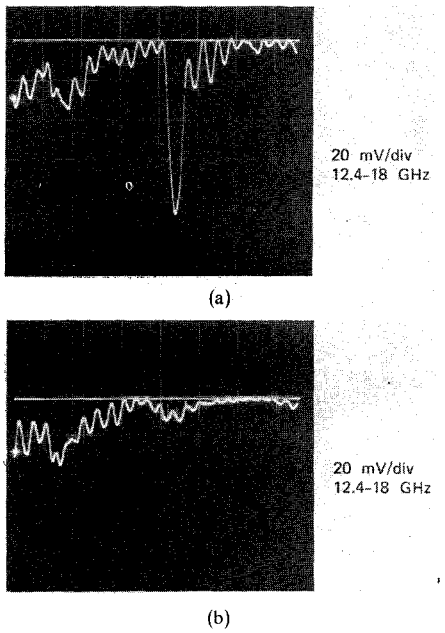

Fig. 6. Reflection property of a grating filter. The values of h_1, h_2, ε_1, and ε_2 are the same as in Fig. 5. (a) Filter with $d = 6.25$ mm, $a = 1.59$ mm, $b = 3.16$ mm, number of grating elements = 30. (b) No grating for reference purposes.

left unradiated beyond the last grating element. To avoid reflection, the forward end of the antenna has a tapered section that unintentionally works as a surface-wave antenna. Although some absorbing materials were placed in front of the tapered termination, not all the undesired radiation was suppressed. It should be relatively straightforward to reduce the effect mentioned here by increasing the length of the antenna and creating more grating cells. By doing this, almost all the energy will radiate as a leaky wave, leaving a negligible amount at the end of the antenna. At the same time, the radiation pattern will be improved because of the increased number of grating elements.

Another source of discrepancy is the transition between the rectangular metal waveguide and the IS guide. A certain amount of radiation contributes the observed radiation-pattern degradation.

By proper choice of d, the grating can be made to reflect incoming signals at frequencies at which (4) is satisfied. Such an arrangement can be applied for realizing a band-reject filter. One example is shown in Fig. 6.

Because the present configuration does not allow measurement of transmission characteristics of the band-reject filter, its reflection properties are measured instead. Fig. 6(a) shows the reflection from a 30-element grating filter. The sharp dip around 15.55 GHz corresponds to the stop band. The cross-sectional dimensions of the IS guide and the grating profile of the filter are identical to those of the antenna, except that d is much smaller in the filter case to satisfy (4).

Fig. 6(b) depicts the reflection from an IS waveguide with dimensions identical to those for Fig. 6(a) but without any grating, and thus serves as a reference for Fig. 6(a). In these figures, the magnitude of reflected signals is measured in the downward direction from the zero level indicated by white horizontal straight sweeps. The bandwidth of the stopband as measured is about 500 MHz, with the center frequency of 15.55 GHz. The return loss of the filter is about 4 dB. However, this value includes the radiation loss at the transition between the IS guide and the open-ended metal waveguide. In a round trip of the wave the radiation loss at the transition is estimated to be 2–3 dB. Hence, the true return loss due to the grating is estimated to be 1–2 dB.

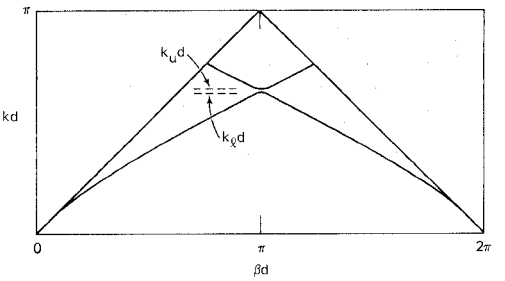

Fig. 7. Dispersion plot illustrating stopband phenomena. Parameters used in computation correspond to those in Fig. 6(a).

Stopband characteristics have been computed by using (5). Dispersion characteristics so obtained are depicted in Fig. 7. From the computed values of $k_u d$ and $k_l d$, the width of the stopband was found to be 300 MHz. The center frequency was 15.25 GHz. The attenuation factor αd at the center frequency was 0.04, which gives rise to the return loss of 0.46 dB for the grating under consideration.

The difference between theoretically and experimentally determined center frequencies is well within the experimental accuracy. The discrepancies between predicted and measured data for the other two parameters are attributed partly to experiments (transmission loss in the IS guide, fabrication irregularity of the grating, etc.), and partly to the use of oversimplified theory described in this paper.

IV. Conclusion

We have demonstrated for the first time that grating structures can be used as antennas and filters for millimeter-wave integrated circuits. Leaky-wave antennas of the type demonstrated can be implemented in the dielectric millimeter IC and can be efficiently coupled with a transmitter or a receiver front end. These antennas are planar and frequency-scannable, and do not require a radome.

Grating type filters of the kind demonstrated are suitable for a number of applications. For instance, by the use of their frequency-sensitive reflection properties, two of the gratings separated by an appropriate distance could be employed as a resonator. Alternatively, two band-reject filters can be combined with a 3-dB hybrid to produce a bandpass filter.

The experimental results agree reasonably well with theoretical predictions. Therefore, it appears that accurate design procedures can be developed without undue difficulty.

We plan to repeat the present work at 60 and 95 GHz where the components described here are more useful. Smaller wavelengths work to our advantage. For instance, radiation of leaky-wave antennas can be improved by making the electrical length larger than the direct scaling of the present 15-GHz model, for the same or even smaller physical size.

References

[1] K. Ogawa, W. S. C. Chang, B. Sopori, and F. J. Rosenbaum, "A theoretical analysis of etched grating couplers for integrated optics," *IEEE J. Quantum Electron.*, vol. QE-9, pp. 29–42, Jan. 1973.

[2] S. Wang, "Principles of distributed feedback and distributed Bragg-reflection lasers," *IEEE J. Quantum Electron.*, vol. QE-10, pp. 413–427, Apr. 1974.

[3] T. Itoh, "Inverted strip dielectric waveguide for millimeter-wave integrated circuits," *IEEE Trans. Microwave Theory Tech.*, vol. MTT-24, pp. 821–827, Nov. 1976.

[4] R. Rudokas and T. Itoh, "Passive millimeter-wave IC components made of inverted strip dielectric waveguides," *IEEE Trans. Microwave Theory Tech.*, vol. MTT-24, pp. 978–981, Dec. 1976.

[5] H. Jacobs and M. M. Chrepta, "Electronic phase shifter for millimeter-wave

semiconductor dielectric integrated circuits," *IEEE Trans Microwave Theory Tech.*, vol. MTT-22, pp 411–417, Apr. 1974.
[6] R. M Knox and P. P. Toulois, "A V-band receiver using image line integrated circuits," *Proc Nat. Electronics Conf.*, vol 27, pp. 489–492, Oct. 1974
[7] H. Jacobs, G Novick, C. M. LoCascio, and M. M. Chrepta, "Measurement of guided wavelength in rectangular dielectric waveguides," *IEEE Trans Microwave Theory Tech.*, vol MTT-24, pp 815–820, Nov. 1976.
[8] R. E Collin and F. J. Zucker, *Antenna Theory*, vol 2 New York: McGraw-Hill, 1969, ch 19, 20
[9] R E. Collin, *Field Theory of Guided Waves*, ch 9 New York: McGraw-Hill, 1960

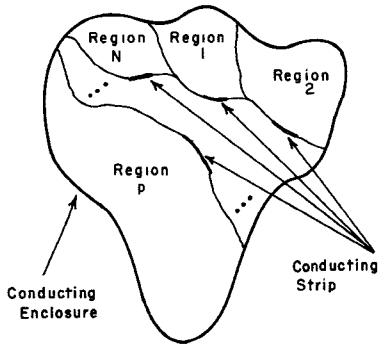

Fig 1. Generic cross section of mixed conductors and dielectrics in conducting enclosure

Dispersion Characteristics for Arbitrarily Configured Transmission Media

ACHINTYA K. GANGULY AND
BARRY E. SPIELMAN, MEMBER, IEEE

***Abstract*—A method for calculating the propagation characteristics of electromagnetic waves along arbitrarily configurated transmission media composed of conductors and/or inhomogeneous dielectrics is presented. The method is based on the equivalence principle. The dispersion characteristics of the fundamental as well as higher order modes can be obtained by this method. To demonstrate the validity of this method, results of the propagation constant of a shielded microstrip line calculated by this method are compared with other numerical results available in the literature. New results for the dispersion characteristics of a channelized suspended microstrip are presented.**

I. Introduction

The success of microstrip in microwave integrated-circuit applications has caused considerable interest in the calculation of dispersion characteristics of these lines. A number of different techniques [1]–[4] have been employed to obtain dispersive effects of open and shielded microstrip-like transmission lines with rectangular cross sections. Since microstrip becomes lossy and difficult to fabricate at higher microwave frequencies, attention has focused on configuring new transmission media. In this short paper we present a technique for calculating the dispersion characteristics of electromagnetic wave propagation along guiding structures consisting of a finite number of uniform dielectric regions of arbitrary cross sections within a conducting enclosure. Conducting strips may also be present at the interface between two dielectric regions. It is assumed that the thickness of the conductors is negligible.

In Section II the problem is formulated on the basis of the equivalence principle. A set of linear integro-differential operator equations for the equivalent current sources are obtained by applying the appropriate boundary conditions at each interface. In Section III the method for converting the operator equations into a matrix formulation by the method of moments [6, pp. 9–11, 14, 15] is sketched. The numerical methods used to determine the propagation characteristics and results for specific examples are described in Section IV.

Manuscript received May 20, 1977; revised July 13, 1977
The authors are with the Naval Research Laboratory, Washington, DC 20375.

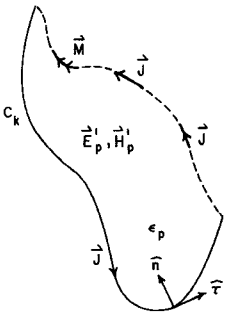

Fig 2 Conceptual treatment of currents and fields for the pth region $\hat{\tau}$, $\hat{n}$, and $\hat{z}$ are unit vectors along three orthogonal coordinates axes used in the text $\hat{z}$ is normal to the plane of the paper pointing up.

II. Integro-Differential Equations

Fig. 1 shows the generic cross section of the guiding structure under consideration. N is the number of discrete, homogeneous, isotropic, dielectric regions inside the conducting enclosure. The heavy lines on the interface between two dielectric regions denote conducting strips. The electric ($\boldsymbol{E}$) and magnetic ($\boldsymbol{H}$) fields in each region will be obtained by applying the principle of equivalence [5]. In accordance with this principle, the dielectric medium of the pth region (characterized by permittivity ε_p) is fictitiously extended to fill all space and combinations of electric ($\boldsymbol{J}^p$) and magnetic ($\boldsymbol{M}^p$) surface current sources are conceptually placed on the boundary S_p of the pth region. $\boldsymbol{J}^p$ and $\boldsymbol{M}^p$ are to be determined in such a way that $\boldsymbol{E}$ and $\boldsymbol{H}$ are zero everywhere outside S_p and are identical to the fields $\boldsymbol{E}^p$ and $\boldsymbol{H}^p$ at each point in the interior of the pth region for the original problem shown in Fig. 1. This procedure is repeated for each of the regions inside the conducting enclosure. The current sources for the various regions are not all independent because of the boundary conditions to be satisfied at all the interfaces. Fig. 2 symbolically shows the contour of the pth region and the surface current distributions on it. $\boldsymbol{M}^p$ is taken to be zero on the conducting segments of the boundary. Also shown in Fig. 2 is a left-handed coordinate system with unit vectors $\hat{\tau}_p$, $\hat{n}_p$, and $\hat{z}$. $\hat{\tau}_p$ is tangential to the contour c_p (counterclockwise), $\hat{n}_p$ inward drawn normal to the region p, and $\hat{z}$ perpendicular to the plane of Fig. 2. For two adjacent regions p and p', we have $\hat{\tau}_p = -\hat{\tau}_{p'}$ and $\hat{n}_p = -\hat{n}_{p'}$ on the portion of boundary common to both the contours c_p and $c_{p'}$. $\hat{z}$ is the same for all regions. Since $\boldsymbol{J}^p$ and $\boldsymbol{M}^p$ are surface currents, we have the relations

$$\hat{n}_p \cdot \boldsymbol{M}^p = 0$$
$$\hat{n}_p \cdot \boldsymbol{J}^p = 0. \tag{1}$$